Importance of oxygen octahedra tilts for the electron-phonon coupling in K-doped $BaBiO_3$

Timur Bazhirov, Sinisa Coh, Steven G. Louie, and Marvin L. Cohen
Department of Physics, University of California at Berkeley, Berkeley, California 94720, USA
and Materials Sciences Division, Lawrence Berkeley National Laboratory, Berkeley, California 94720, USA
(Received 17 October 2013; published 20 December 2013)

Despite considerable research efforts, a clear understanding of superconductivity in $Ba_{0.5}K_{0.5}BiO_3$ has been elusive. Recent studies showed that although electron-correlation effects in this compound can significantly increase the electron-phonon coupling, they do not reproduce the measured Eliashberg spectral function (α^2F). We show that the oxygen octahedra tilts in $Ba_{0.5}K_{0.5}BiO_3$ increase α^2F in the range of frequencies near 30 meV, even on the level of the generalized gradient approximation. This increase in α^2F changes its shape to provide better agreement with experiment and results in a 50–60% increase of the average electron-phonon coupling strength λ. We use the Wannier interpolation technique to determine the electron-phonon coupling with high precision.

DOI: 10.1103/PhysRevB.88.224509 PACS number(s): 74.20.Pq, 71.38.−k, 63.20.kd

I. INTRODUCTION

More than two decades ago it was found[1,2] that the superconducting transition temperature T_c of $Ba_{1-x}K_xBiO_3$ is close to 30 K (for $x = 0.4$), one of the highest among materials without copper or iron. Unlike copper- and iron-based superconductors, $Ba_{1-x}K_xBiO_3$ is nonmagnetic,[2,3] and its electrons are likely paired by a more conventional electron-phonon coupling mechanism. A large value of electron-phonon coupling parameter λ (about 1.0–1.2) was confirmed by the tunneling measurements,[4,5] as well as by specific heat experiments.[6] This large electron-phonon coupling has been suggested to originate from proximity to the charge-density-wave phase[7–12] in the parent compound ($BaBiO_3$) and the accompanied Bi-O breathing structural distortion.[13]

There are several theoretical studies of the origin of superconductivity in $Ba_{1-x}K_xBiO_3$. An early study of the Bi-O breathing mode on the basis of the frozen-phonon approximation estimated λ to be about 0.3 based on this mode,[14] much smaller than the experimental value (1.0–1.2). A more detailed calculation, using the virtual crystal approximation (VCA) and including all phonon branches sampled over the Brillouin zone, gave nearly the same value of $\lambda = 0.3$.[15] Even the inclusion of anharmonic effects cannot account for the discrepancy between theory and experiment. The additional anharmonic contribution[15] to λ is estimated to be 0.04.[16]

To account for the differences between experiment and theory, recent studies[18,19] emphasized shortcomings of the local-density approximation (LDA) to describe the electron correlation. A study based on the GW approximation and hybrid functionals in Ref. 19 found the shift of the electronic bands due to a Bi-O breathing mode to be $\sim\sqrt{3}$ times larger than for LDA. The authors then performed *ad hoc* rescaling of the Brillouin-zone average LDA electron-phonon coupling parameter, obtained in the VCA case ($\lambda \approx 0.3$), by a factor of $\sim$3 which yielded $\lambda = 1$.

Approaching from a different perspective, we found in the current work that a careful treatment of structural distortions increases the spectral weight in the low- and mid-frequency zone of the Eliashberg spectral function α^2F. This increase leads to a better correspondence between theory and experiment. A sketch of how the hybrid functional approach from Ref. 19 and the structural distortions considered in this work adjust the VCA result for α^2F is given in Fig. 1. We have not attempted to use the hybrid functionals approach as it would make an extensive study of phonon and electron-phonon coupling properties not feasible computationally within our model of including the structural distortions and doping explicitly.

In this paper we show that presence of oxygen octahedra tilts[20] in $Ba_{0.5}K_{0.5}BiO_3$ increases λ from 0.3 to 0.45, even on the level of a conventional generalized gradient approximation. We also explicitly include dopant atoms (K) in our calculation, without relying on the virtual crystal approximation. In addition, we use Wannier interpolation techniques[21] to integrate the electron-phonon coupling on a very fine mesh in the Brillouin zone (mesh size is up to $30 \times 30 \times 30$).

The paper is arranged as follows: Sec. II explains the methods and the computational details, Sec. III contains the results, and in Sec. IV we discuss our findings and relate them to the previous studies. Finally, we present conclusions in Sec. V.

II. METHODS

In this work we use the generalized gradient approximation (GGA) to the density functional theory (DFT)[22,23] within a plane-wave pseudopotential scheme[24–26] as implemented in Quantum ESPRESSO.[27] Scalar-relativistic norm-conserving pseudopotentials with a plane-wave basis up to 80 Ry are employed. For the valence states in the pseudopotential for Bi we use $5d$, $6s$, and $6p$ states; for Ba, $5s$, $5p$, $6s$; for O, $2s$, $2p$; for K, $3s$, $3p$, $4s$. We find that inclusion of semicore states is important to correctly reproduce structural distortions in $Ba_{1-x}K_xBiO_3$.

Density-functional perturbation theory[28] is used to compute phonon frequencies $\omega_{\vec{Q},\nu}$ and electron-phonon coupling parameters $\lambda_{\vec{Q},\nu}$ on a coarse mesh ($4 \times 4 \times 4$ in the 20-atom cell case, $6 \times 6 \times 6$ for the five-atom cell) of reciprocal vectors $\vec{Q}$ (ν is the phonon branch index). Next, interpolation techniques[21] based on maximally localized Wannier functions[21,29,30] are used to interpolate electron-phonon coupling parameters on a fine grid (up to $30 \times 30 \times 30$). For

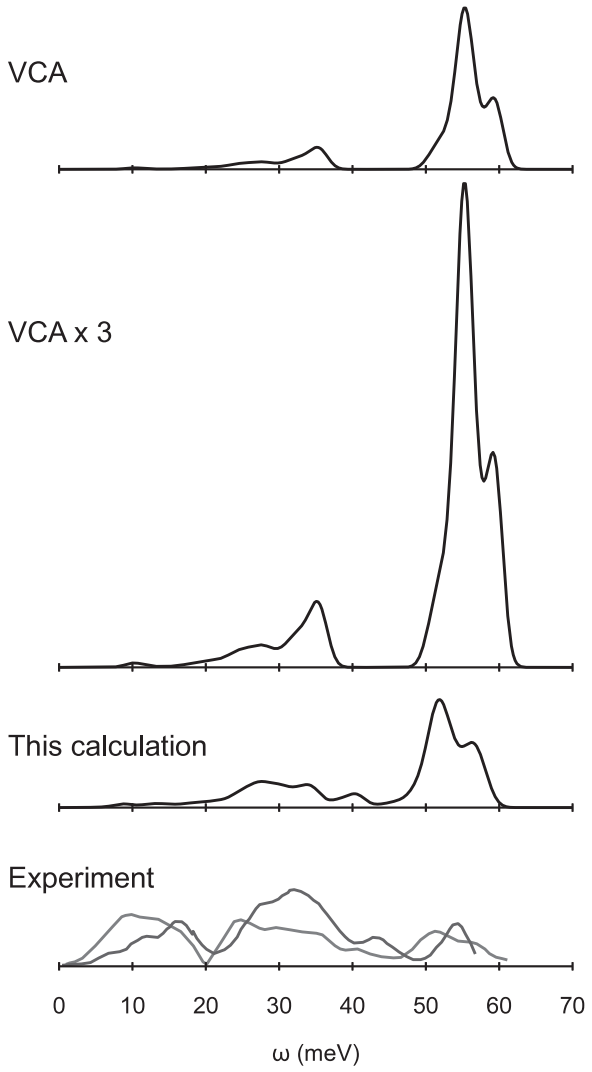

FIG. 1. Hybrid functionals (Ref. 19) give an overall threefold increase of the VCA spectral function [$\alpha^2F(\omega)$]. Our work shows that the octahedral rotations, even on the GGA level, transfer spectral weight towards lower frequencies (from ∼55 to ∼30 meV). The experimental results are taken from Ref. 4.

this interpolation, the Wannier90 and EPW packages are employed.[31,32]

Once we have the interpolated phonon frequencies and electron-phonon coupling, the Eliashberg spectral function $\alpha^2F(\omega)$ is computed by integration over the Brillouin zone:

$$\alpha^2F(\omega) = \frac{1}{2}\sum_{\vec{Q},\nu}\omega_{\vec{Q},\nu}\lambda_{\vec{Q},\nu}\delta(\omega-\omega_{\vec{Q},\nu}). \quad (1)$$

Using Eq. (1), the frequency moments of the Eliashberg spectral function are extracted and the average coupling λ is computed:

$$\lambda = 2\int \omega^{-1}\alpha^2F(\omega)d\omega = 1/N\sum_{\vec{Q},\nu}\lambda_{\vec{Q},\nu}, \quad (2)$$

where N is the total number of points on a $\vec{Q}$ grid in the Brillouin zone. Finally, λ is used in the McMillan equation[33]

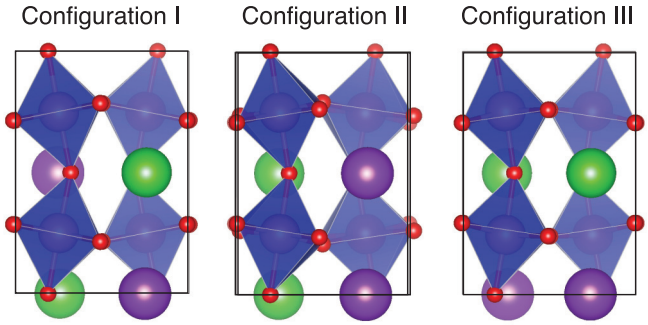

FIG. 2. (Color online) Three possible arrangements of the dopant atoms (K) in the 20-atom primitive unit cell of $Ba_{0.5}K_{0.5}BiO_3$. Atomic colors are O: red; K: purple; Ba: green. Bi atoms are inside blue octahedra. All projections are along 110 direction (same as dominant octahedral tilt).

to estimate the superconducting transition temperature T_c as

$$T_c = \frac{\omega_{\log}}{1.20}\exp\left[-\frac{1.04(1+\lambda)}{\lambda-\mu^*(1+0.62\lambda)}\right]. \quad (3)$$

Here $\omega_{\log}$ is the logarithmic average of the phonon frequencies and μ^* is the Coulomb repulsion parameter. For μ^* we use a standard value of 0.1, as well as $\mu^* = 0$ to test the value of T_c for a best-case scenario.

III. RESULTS

A. Atomic structure

In this work we use the fully relaxed structure of $Ba_{0.5}K_{0.5}BiO_3$ in the enlarged primitive unit cell containing 20 atoms ($\sqrt{2}\times\sqrt{2}\times 2$ reconstruction of the primitive cubic five-atom cell). In addition, we explicitly take into account dopant atoms (K) and do not rely on the virtual crystal approximation. We consider all three possible arrangements of the dopant atoms (K) in the 20-atom primitive unit cell of $Ba_{0.5}K_{0.5}BiO_3$. These configurations, labeled I, II, III, consist of alternating planes of K and Ba atoms along [111], [110], and [001] directions respectively (see Fig. 2). The three doping arrangements are within 50 meV (per formula unit) from each other in energy with total energies decreasing from I to III.

For an easier comparison with previous theoretical work, we also treat $Ba_{0.5}K_{0.5}BiO_3$ using the virtual crystal approximation (VCA), in a simple cubic five-atom unit cell. In addition, we fully relax the structure of the parent compound ($BaBiO_3$) in the same enlarged unit cell ($\sqrt{2}\times\sqrt{2}\times 2$) as for the doped compound.

The summary of the structural parameters for all systems studied in this work is given in Table I. In the case of the undoped parent compound ($BaBiO_3$) we find that the fully relaxed structure has two kinds of structural distortions. First, there is a Bi-O breathing distortion which reduces the Bi-O bond length for half of the Bi atoms (4.19 bohrs), and increases it for the other half (4.39 bohrs). Second, there is a tilt of oxygen octahedra around both [110] and [001] directions (13.4° and 6.5°). Our calculation is in good agreement both for Bi-O breathing and octahedral tilt with the experimental data. The

TABLE I. Structural parameters of $BaBiO_3$ and $Ba_{0.5}K_{0.5}BiO_3$. For $Ba_{0.5}K_{0.5}BiO_3$ we show results for three different configurations of dopant (K) atoms (configurations I, II, and III), as well as for the virtual crystal approximation (VCA). Experimental data are shown in parentheses (Refs. 3 and 20). This table shows the equilibrium unit-cell volume V (in Å^3 per formula unit of $Ba_{0.5}K_{0.5}BiO_3$), the maximum and minimum Bi-O bond lengths (in bohrs) and octahedral tilt angles along [110] and [001] directions (in deg).

		Bi-O bond length		Octahedral tilt	
	V (Å^3)	Min. (bohrs)	Max. (bohrs)	[110] (deg)	[001] (deg)
$BaBiO_3$					
	87.02	4.19	4.39	13.4	6.5
	(82.21)	(4.01)	(4.19)	(12)	(6)
$Ba_{0.5}K_{0.5}BiO_3$					
Config. I	82.74	4.16	4.18	10.7	1.4
Config. II	83.02	4.16	4.18	8.8	2.6
Config. III	83.09	4.11	4.23	9.0	1.1
VCA	84.65	4.15	4.15		
	(77.41)	(4.03)	(4.03)	(4.5)[a]	

[a]The experimental study in Ref. 20 was unable to determine direction of the oxygen octahedra tilts.

unit-cell volume is overestimated by 6% as compared to the experiment, as is commonly found in the GGA approximation.

The fully relaxed doped structure ($Ba_{0.5}K_{0.5}BiO_3$) has an almost negligible amount of Bi-O breathing distortion, unlike the parent compound. However, the doped compound still has a significant amount of octahedral tilts, especially around the [110] axis (between 8.8° and 10.8°). The amount of tilt along the [001] axis is small: about 1–2°. The bond lengths and tilts obtained for the undoped compound are in good agreement with the results of previous calculations[7,8,18,34] and experimental data. Our calculations show that the unit-cell volume of the doped structure is 5% lower than the volume of the parent compound. This is, again, in good agreement with experimental observation (6% lower).

B. Electronic structure

The electronic band structures and the densities of states (DOS) for all studied configurations are given in Fig. 3. The parent compound ($BaBiO_3$) is experimentally found to have a semiconducting gap of 0.2 eV.[35] However in our GGA calculations, as well as in the previous theoretical studies,[8,14,18] the parent compound is slightly semimetallic (conduction-band minimum is 0.3 eV below the Fermi level). The width of the valence band is 0.9 eV and it has mostly oxygen $2p$ character (see right panels in Fig. 3). More extensive treatments of electronic correlation effects are able to reproduce semiconducting behavior of the parent compound.[18]

The K-doped compound ($Ba_{0.5}K_{0.5}BiO_3$) is metallic in our calculation. The overall shape of the valence band is similar to that in the parent compound. However, the Fermi level (relative to the valence-band maximum) is downshifted by 0.5–0.7 eV, and the width of the band is increased from 0.9 to 1.6 eV. Additionally, there is a series of band splittings on the order of

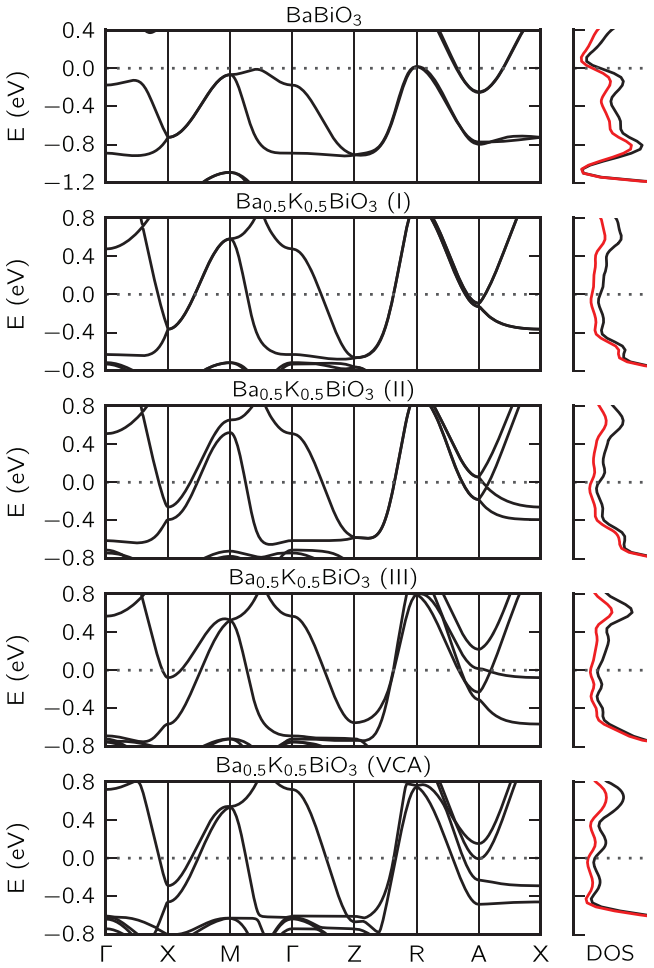

FIG. 3. (Color online) The electron band structure for a parent compound ($BaBiO_3$) and a doped compound ($Ba_{0.5}K_{0.5}BiO_3$) with different configurations of dopant atoms (I, II, and III, see Sec. III A). For comparison we also show the band structure using the virtual crystal approximation (VCA) in the folded Brillouin zone. Total densities of states (black) and the oxygen $2p$ partial density of states (red) are given in the small panel on the right.

0.1–0.2 eV at the A and X points of the Brillouin zone. These splittings are present only for configurations II and III of the dopant atoms, while they nearly disappear in the configuration I during the structural relaxation. The band character of the valence band in the doped compound is oxygen $2p$, the same as in the case of the parent compound. The total density of states at the Fermi level varies within 5–10% between configurations I, II, and III.

For comparison with earlier studies, we also calculate the band structure using the VCA. Overall, we find that the band structure of $Ba_{0.5}K_{0.5}BiO_3$ in the VCA has a similar (within 10%) bandwidth and density of states at the Fermi level as in our full 20-atom calculation. We find good agreement with previous similar studies regarding the band structures and partial densities of states.[2,8,14,18]

C. Phonons

The experimental and theoretical phonon densities of states for the doped compound are shown in the top four

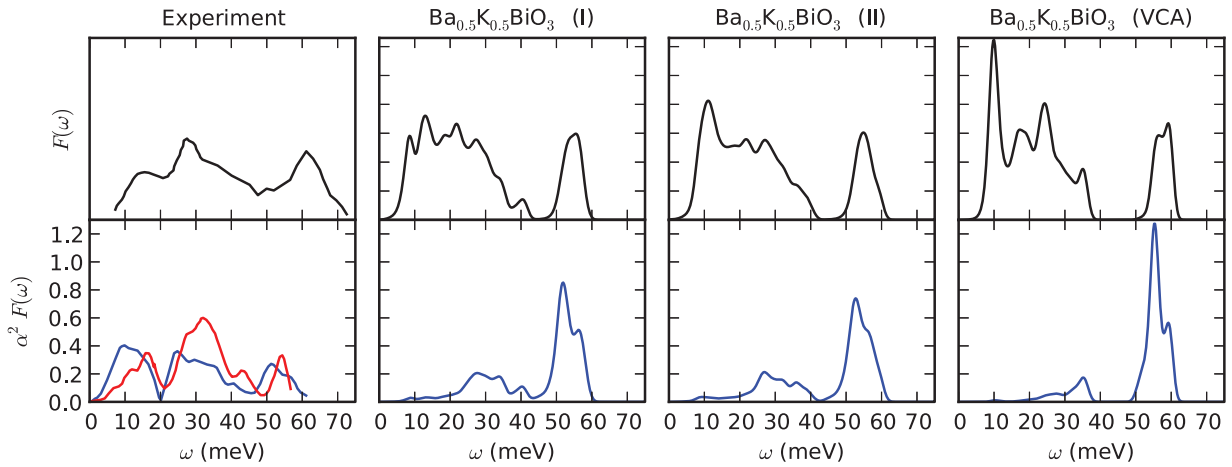

FIG. 4. (Color online) The phonon densities of states $F(\omega)$ (black, upper panel) and the Eliashberg spectral functions $\alpha^2F(\omega)$ (blue and red, lower panel). The experimental phonon density of states is from Ref. 4 and corresponds to $Ba_{1-x}K_xBiO_3$ with $x = 0.4$. Two measured Eliashberg spectral functions (red and blue) are from the same Ref. 4 and they correspond to $x = 0.375$. We also show calculated $F(\omega)$ and $\alpha^2F(\omega)$ from this work ($x = 0.5$) for the configuration of dopant atoms I and II (see Sec. III A), as well as the calculation using virtual crystal approximation. The $F(\omega)$ is given in arbitrary units so that area under the curve is the same in each panel.

panels of Fig. 4. Our theoretical calculation shows that the intensity of the phonon density of states is concentrated in a broad low-energy region (10–40 meV) and in a narrower higher-energy region (55–60 meV). Small differences with respect to experiment are likely due to the equilibrium volume overestimation of our GGA calculation. In our calculations, the low-energy region consists of the movement of the heavier atoms (Ba, K, Bi) with an admixture of oxygen displacement. The high-energy region is dominated by the oxygen modes.

For a comparison with earlier studies we also calculated the phonon density of states using the virtual crystal approximation (VCA). We find a strong peak in the phonon density of states near 10 meV that is not present in our fully relaxed 20-atom unit-cell calculation, or in experiment. In addition, the VCA overestimates the gap in the phonon density of states (near 45 meV). The gap separates the phonon modes involving the O-octahedra breathing at 55 meV from the rest.

We also studied the phonons of the undoped parent compound (not shown in Fig. 4) and find that it does not have a gap in the phonon density of states in agreement with experimental finding.[9,10]

D. Electron-phonon coupling

The experimental and theoretical Eliashberg spectral functions α^2F [Eq. (1)] are shown in the bottom panels of Fig. 4. Experimental spectral function has a peak at ∼10–20, ∼30, and ∼55 meV. The 30- and 55-meV peaks are present in our fully relaxed 20-atom cell calculation, but with different magnitudes. In addition, α^2F is nearly zero at frequencies below 20 meV, unlike in the experiment.

The virtual crystal approximation (VCA) calculation of α^2F disagrees even more with the experiment. The middle peak (at 30 meV) is lower than in our fully relaxed calculation while the high-energy peak (at 55 meV) is higher. The lowering of the spectral function near 30 meV is also responsible for a lower average electron-phonon coupling λ [Eq. (2)] in VCA.

Figure 5 shows the electron-phonon coupling $\lambda_{\vec{Q}} = \sum_\nu \lambda_{\vec{Q},\nu}$ and the nesting function along a path inside the phonon Brillouin zone. The nesting function serves as a measure of how many potential electron scattering states are present at a particular wave vector $\vec{Q}$,[37]

$$\xi_{\vec{Q}} = \frac{1}{N_k}\sum_{\vec{k}} \delta(\epsilon_{\vec{k}})\delta(\epsilon_{\vec{k}+\vec{Q}}). \quad (4)$$

Above N_k is the total number of $\vec{k}$ vectors included in the sum and $\delta(\epsilon_{\vec{k}})$ is the Dirac δ function.

In all of our calculations, the nesting function is nearly proportional to the electron-phonon coupling $\lambda_{\vec{Q}}$. Therefore, the strength of the electron-phonon interaction varies slowly throughout the phonon Brillouin zone.

E. Superconducting parameters

Table II gives the parameters used in our estimate of the superconducting transition temperature T_c. Shown are the square ($\sqrt{\langle\omega^2\rangle}$) and the logarithmic average ($\omega_{\log}$) frequency moments of the Eliashberg spectral function, and the average electron-phonon coupling strength λ. We estimate the superconducting transition temperature using the McMillan formula[33] [Eq. (3)]. In the table we show the estimated T_c using a Coulomb parameter $\mu^* = 0.0$ and 0.1.

Using a fully relaxed 20-atom cell we obtain $\lambda = 0.45$ in configuration I and $\lambda = 0.48$ in configuration II. These values produce T_c estimates of 4.2 and 3.2 K for $\mu^* = 0.1$ (14 and 12 K for $\mu^* = 0$). For the 20-atom case the logarithmic average frequency is 384 K in configuration I and 393 K in configuration II.

In the virtual crystal approximation we obtain $\lambda = 0.30$. This leads to a T_c of only 0.5 K for $\mu^* = 0.1$ (and 6.5 K for $\mu^* = 0.0$). The value of the logarithmic average frequency in the VCA is 575 K.

IV. DISCUSSION

The most striking disagreement between the theoretical and experimental Eliashberg spectral function α^2F is coming from

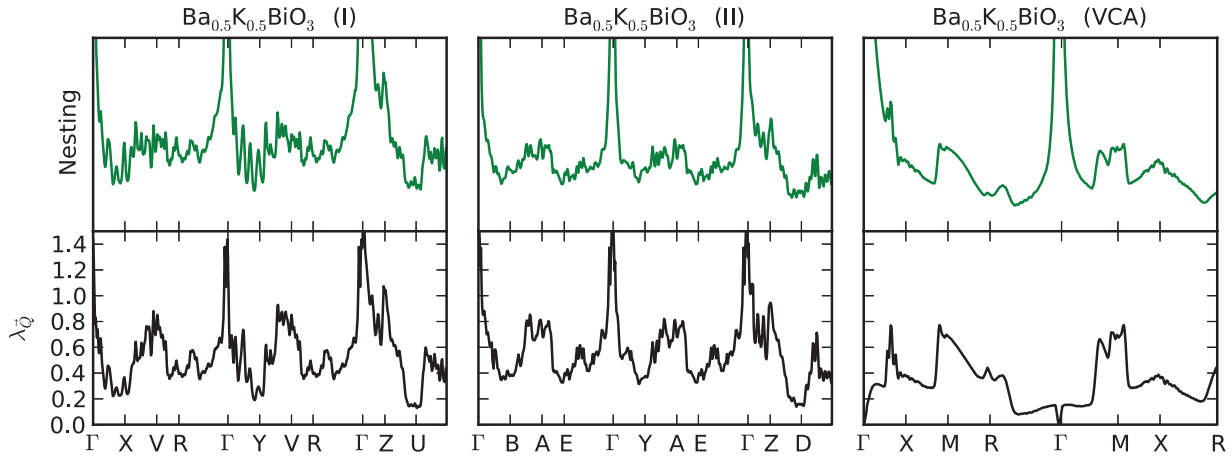

FIG. 5. (Color online) The Fermi-surface nesting function (Refs. 36 and 37) (green, above) and the electron-phonon coupling $\lambda_{\vec{Q}}$ (black, below) along a path in the phonon Brillouin zone. We show results for $Ba_{0.5}K_{0.5}BiO_3$ both in the configurations I and II (see Sec. III A) and for the virtual crystal approximation (VCA). The nesting function is given in arbitrary units. In the plot we impose $\lambda_{\vec{Q},\nu}$ to be equal to zero for small $\vec{Q}$ and ω_ν.

the low-frequency region between 10 and 40 meV (see Fig. 4). The phonon spectrum in this region consists of movement of heavier atoms (Ba, Bi, K) with some admixture of the oxygen movement. The higher region of frequencies (above 40 meV) consists mostly of oxygen-breathing modes, and computed α^2F in that region is larger than in the experiment.

The only first-principle theoretical study with a λ and T_c close to the experimental values is the hybrid-functional calculation from Ref. 19. However, this agreement with experiment is achieved by a threefold increase in the electron-phonon coupling of the high-frequency (55-meV) oxygen-breathing phonon. Therefore this increase is in an opposite direction to what is required to have α^2F in better agreement with experiment. What is needed is that low-frequency (10–40 meV) α^2F increases, and high-frequency α^2F decreases.

Our work shows that the proper treatment of the atomic structure, especially the oxygen octahedra tilts, can increase electron-phonon coupling parameter λ by 50–60%. In addition, this increase comes mostly from an enhancement of the spectral weight for α^2F in the low-frequency regime near 30 meV. Therefore, we propose that a more elaborate electron-correlation study (such as hybrid-functional from Ref. 17 or GW method) together with the proper treatment of the atomic structure may give α^2F in better agreement with experiment. Combined effect of elaborate electron-correlations assessment and proper treatment of the atomic structure need not be simply additive. We also speculate that disorder, present in the spatial arrangement of K atoms, might further increase α^2F in the 10–40-meV range.

TABLE II. Theoretical estimate of the superconducting transition temperature T_c obtained using the McMillan formula (Ref. 33) [Eq. (3)] with a Coulomb parameter μ^* given. We also show the square and logarithmic average frequencies (Ref. 36) ($\sqrt{\langle\omega^2\rangle}$ and $\omega_{\log}$), average electron-phonon coupling strength λ. The results for the doped configuration III (not shown here) were obtained only on a coarse grid $4\times4\times4$ and are within 3–5% of the results for configuration I and II.

	$\sqrt{\langle\omega^2\rangle}$	$\omega_{\log}$		T_c (K)	
	(K)	(K)	λ	$\mu^*=0.1$	$\mu^*=0.0$
$Ba_{0.5}K_{0.5}BiO_3$					
Config. I	480	393	0.48	4.2	14.0
Config. II	479	384	0.45	3.2	12.0
VCA	575	522	0.30	0.5	6.5

V. CONCLUSION

We studied the electronic, phonon, and electron-phonon properties of the $Ba_{0.5}K_{0.5}BiO_3$ superconductor. Unlike the previous studies, we perform calculations in the fully relaxed 20-atom unit cell. We find that the presence of oxygen octahedra tilts increases the average electron-phonon coupling λ by 50–60% (from 0.3 to 0.48) as compared to the more conventionally used virtual crystal approximation (VCA) without tilts. This increase in λ originates from enhanced electron-phonon coupling at intermediate phonon frequencies (near 30 meV), but it is still not large enough to explain the experimentally obtained superconducting transition temperature. We suggest that the agreement may be improved further by an electron-correlation study going beyond the GGA (as in Ref. 19) in combination with the inclusion of the oxygen octahedra tilts.

ACKNOWLEDGMENTS

Structural study and the work on the ground-state properties were supported by NSF Grant No. DMR10-1006184. The electron-phonon properties calculations were supported by the Theory Program at the Lawrence Berkeley National Lab through the Office of Basic Energy Sciences, US Department of Energy, under Contract No. DE-AC02-05CH11231. S.G.L. acknowledges support of a Simons Foundation Fellowship in Theoretical Physics. Computational resources were provided by the National Energy Research Scientific Computing Center, which is supported by the Office of Science of the US Department of Energy.

[1]R. J. Cava, B. Batlogg, J. J. Krajewski, R. Farrow, L. W. Rupp, A. E. White, K. Short, W. F. Peck, and T. Kometani, Nature (London) **332**, 814 (1988).
[2]L. F. Mattheiss, E. M. Gyorgy, and D. W. Johnson, Phys. Rev. B **37**, 3745 (1988).
[3]S. Pei, J. D. Jorgensen, B. Dabrowski, D. G. Hinks, D. R. Richards, A. W. Mitchell, J. M. Newsam, S. K. Sinha, D. Vaknin, and A. J. Jacobson, Phys. Rev. B **41**, 4126 (1990).
[4]Q. Huang, J. F. Zasadzinski, N. Tralshawala, K. E. Gray, D. G. Hinks, J. L. Peng, and R. L. Greene, Nature (London) **347**, 369 (1990).
[5]N. Tralshawala, J. F. Zasadzinski, L. Coffey, W. Gai, M. Romalis, Q. Huang, R. Vaglio, and K. E. Gray, Phys. Rev. B **51**, 3812 (1995).
[6]R. Kuentzler, C. Hornick, Y. Dossman, S. Wegner, R. E. Farsi, and M. Drillon, Physica C: Superconductivity **184**, 316 (1991).
[7]L. F. Mattheiss and D. R. Hamann, Phys. Rev. B **28**, 4227 (1983).
[8]L. F. Mattheiss and D. R. Hamann, Phys. Rev. Lett. **60**, 2681 (1988).
[9]C.-K. Loong, P. Vashishta, R. K. Kalia, M. H. Degani, D. L. Price, J. D. Jorgensen, D. G. Hinks, B. Dabrowski, A. W. Mitchell, D. R. Richards *et al*., Phys. Rev. Lett. **62**, 2628 (1989).
[10]C.-K. Loong, P. Vashishta, R. K. Kalia, W. Jin, M. H. Degani, D. G. Hinks, D. L. Price, J. D. Jorgensen, B. Dabrowski, A. W. Mitchell *et al*., Phys. Rev. B **45**, 8052 (1992).
[11]M. Braden, W. Reichardt, W. Schmidbauer, A. Ivanov, and A. Rumiantsev, J. Supercond. **8**, 595 (1995).
[12]M. Braden, W. Reichardt, S. Shiryaev, and S. Barilo, Physica C: Superconductivity **378–381, Part 1**, 89 (2002).
[13]D. Cox and A. Sleight, Solid State Commun. **19**, 969 (1976).
[14]A. I. Liechtenstein, I. I. Mazin, C. O. Rodriguez, O. Jepsen, O. K. Andersen, and M. Methfessel, Phys. Rev. B **44**, 5388 (1991).
[15]V. Meregalli and S. Y. Savrasov, Phys. Rev. B **57**, 14453 (1998).
[16]Earlier study (Ref. 17) estimated anharmonic λ to be equal to 0.2.
[17]K. Kunc and R. Zeyher, Phys. Rev. B **49**, 12216 (1994).
[18]C. Franchini, A. Sanna, M. Marsman, and G. Kresse, Phys. Rev. B **81**, 085213 (2010).
[19]Z. P. Yin, A. Kutepov, and G. Kotliar, Phys. Rev. X **3**, 021011 (2013).
[20]Y. Yacoby, S. Heald, and E. Stern, Solid State Commun. **101**, 801 (1997).
[21]F. Giustino, M. L. Cohen, and S. G. Louie, Phys. Rev. B **76**, 165108 (2007).
[22]D. M. Ceperley and B. J. Alder, Phys. Rev. Lett. **45**, 566 (1980).
[23]J. P. Perdew, K. Burke, and M. Ernzerhof, Phys. Rev. Lett. **77**, 3865 (1996).
[24]J. Ihm, A. Zunger, and M. Cohen, J. Phys. C **12**, 4409 (1979).
[25]N. Troullier and J. L. Martins, Phys. Rev. B **43**, 1993 (1991).
[26]M. L. Cohen, Phys. Scr. **1982**, 5 (1982).
[27]P. Giannozzi, S. Baroni, N. Bonini, M. Calandra, R. Car, C. Cavazzoni, D. Ceresoli, G. L. Chiarotti, M. Cococcioni, I. Dabo *et al*., J. Phys.: Condens. Matter **21**, 395502 (2009).
[28]S. Baroni, S. de Gironcoli, A. Dal Corso, and P. Giannozzi, Rev. Mod. Phys. **73**, 515 (2001).
[29]N. Marzari and D. Vanderbilt, Phys. Rev. B **56**, 12847 (1997).
[30]I. Souza, N. Marzari, and D. Vanderbilt, Phys. Rev. B **65**, 035109 (2001).
[31]A. A. Mostofi, J. R. Yates, Y.-S. Lee, I. Souza, D. Vanderbilt, and N. Marzari, Comput. Phys. Commun. **178**, 685 (2008).
[32]J. Noffsinger, F. Giustino, B. D. Malone, C.-H. Park, S. G. Louie, and M. L. Cohen, Comput. Phys. Commun. **181**, 2140 (2010).
[33]P. Allen and R. Dynes, Phys. Rev. B **12**, 905 (1975).
[34]L. F. Mattheiss and D. R. Hamann, Phys. Rev. B **26**, 2686 (1982).
[35]A. Sleight, J. Gillson, and P. Bierstedt, Solid State Commun. **17**, 27 (1975).
[36]P. Allen and B. Mitrovic, *Solid State Physics Vol. 32* (Academic, New York, 1982).
[37]D. Kasinathan, J. Kuneš, A. Lazicki, H. Rosner, C. S. Yoo, R. T. Scalettar, and W. E. Pickett, Phys. Rev. Lett. **96**, 047004 (2006).